The impact of westerly wind bursts on the diversity and predictability of El Niño events: An ocean energetics perspective

Shineng Hu[1], Alexey V. Fedorov[1], Matthieu Lengaigne[2], and Eric Guilyardi[2,3]

[1]Department of Geology and Geophysics, Yale University, New Haven, Connecticut, USA, [2]IPSL/LOCEAN (Sorbonne Universités, UPMC-CNRS-IRD-MNHN), Paris, France, [3]NCAS Climate, Meteorology Department, University of Reading, Reading, UK

Abstract In this study, we apply ocean energetics as a diagnostic tool to investigate the impact of westerly wind bursts (WWBs) on the evolution, diversity, and predictability of El Niño events. Following Fedorov et al. (2014), we add an observed WWB to simulations within a comprehensive coupled model and explore changes in the available potential energy (APE) of the tropical Pacific basin. We find that WWB impacts strongly depend on the ocean initial state and can range from a Central Pacific (CP) to Eastern Pacific (EP) warming, which is closely reflected by the ocean energetics. Consequently, the APE can be used to quantify the diversity of El Niño events within this continuum—higher negative APE values typically correspond to EP events, lower values to CP events. We also find that a superimposed WWB enhances El Niño predictability even before the spring predictability barrier, if one uses the APE as a predictor.

1. Introduction

The El Niño–Southern Oscillation (ENSO) is the dominant mode of climate variability in the tropical Pacific with pronounced global teleconnections [e.g., *Philander*, 1990; *Sarachik and Cane*, 2010]. Recently, the diversity of El Niño events has attracted strong attention [*Ashok et al.*, 2007; *Kao and Yu*, 2009; *Kug et al.*, 2009; *Lee and McPhaden*, 2010; *Yeh et al.*, 2009]. Specifically, a number of studies distinguish between the Central Pacific (CP) El Niño events with the maximum sea surface temperature (SST) anomaly in the central Pacific and the Eastern Pacific (EP) El Niño events with the maximum SST anomaly in the eastern Pacific. Other terminology is also used (Warm Pool El Niño versus Cold Tongue El Niño; El Niño Modoki versus conventional El Niño, etc.). However, debates continue on whether the two El Niño "flavors" involve different physics or whether they represent a continuum of events [e.g., *Cai et al.*, 2014; *Fedorov et al.*, 2014; *Karnauskas*, 2013; *Lengaigne and Vecchi*, 2010; *Ray and Giese*, 2012; *Takahashi et al.*, 2011].

Westerly wind bursts (WWBs) sporadically occur in the western tropical Pacific near the date line and are believed to play an important role in ENSO dynamics, modulating the strength or timing of El Niño events [*Fedorov*, 2002; *Fedorov et al.*, 2003; *Kessler*, 2002; *Lengaigne et al.*, 2004; *McPhaden*, 1999; *McPhaden and Yu*, 1999]. The duration of WWBs ranges from several days to 1–2 months, and their spatial scale can extend to several thousand kilometers [*Harrison and Vecchi*, 1997]. The recent study of *Fedorov et al.* [2014], looking on the development of El Niño events after a superimposed WWB in a coupled model, suggests that the exact same WWB can induce a variety of events ranging from extreme EP events to weak CP events or lead to no warming at all, depending on the ocean initial state at the moment of the wind burst. Thus, WWBs can potentially contribute to the El Niño diversity.

Recently, ocean energetics emerged as a powerful diagnostic tool for studying variability and ocean-atmosphere interactions in the tropical Pacific and Atlantic [*Brown and Fedorov*, 2010; *Brown et al.*, 2011; *Burls et al.*, 2012; *Fedorov*, 2002, 2007; *Fedorov et al.*, 2003; *Goddard and Philander*, 2000]. The ocean energetics describes the rate of change of the Available Potential Energy (APE or *E* for simplicity) induced by buoyancy power generated by the divergence of surface wind-driven currents, which in turn is related to wind power (*W*). Mathematically, the APE balance can be represented as

$$\frac{\partial E}{\partial t} = \gamma W - \text{Dissipation} \tag{1}$$

where γ is the efficiency of energy transfer from surface winds to the ocean thermocline (close to 50%, see *Brown and Fedorov* [2010]). A wind burst modifies wind power and hence the APE. In ENSO studies, this budget is typically computed for the tropical Pacific basin (section 3). One could integrate this equation and neglect dissipation to obtain

$$E_{\text{final}} \approx E_{\text{initial}} + \gamma \int W \, dt \qquad (2)$$

The integral in equation (2) describes the total work generated by the winds and is affected by E_{initial}, the WWB if imposed, and the subsequent wind anomalies.

In the present study, we analyze the same numerical experiments as in *Fedorov et al.* [2014] but focus on different scientific objectives while using a different methodology (ocean energetics). In particular, the ocean energetics provides a tool to quantify El Niño diversity and also helps to shed light on the impact of WWBs on El Niño predictability. We show that a timely WWB can enhance El Niño predictability, even when the prediction is made before the spring predictability barrier (i.e., the rapid decline of SST persistence after April, see *Clarke and Van Gorder* [1999], *McPhaden* [2003], and *Torrence and Webster* [1998]).

2. Model, Experiments, and Data

HadOPA, the comprehensive coupled general circulation model used in our study, couples the OPA ocean model and the HadAM3 atmosphere model. For the OPA, the horizontal resolution is 2° by 2° globally and refined to 0.5° in the meridional direction toward the equator. There are 31 vertical levels with the highest resolution (10 m) in the upper 150 m, and the lowest (500 m) in the deep ocean. The HadAM3 atmosphere model has the 3.75°×2.5° resolution in longitude and latitude, and 19 vertical levels with the higher resolution near the surface and the tropopause.

HadOPA represents the mean tropical climate with high fidelity, having a robust ENSO with a period of 3 to 4 years. Shortcomings of the model, when compared to the observations, include a stronger mean east-west SST gradient along the equator and a stronger variance of the Niño3 index (by approximately 30% for the control run). These issues are due to the relatively strong sensitivity of zonal winds to SST anomalies in the model. More details can be found in *Lengaigne et al.* [2004, 2006], and *Fedorov et al.* [2014].

We conduct two sets of ensemble experiments, with initial conditions chosen from the last 100 years of the long spin-up simulation. In Set 1, the initial ocean heat content (OHC) is recharged (higher by 0.5°C than the model climatology), while in Set 2 it is neutral (OHC anomaly is near zero). The OHC is defined as temperature averaged between 0 and 300 m depth, 5°S–5°N and 120°E–70°W. Therefore, we refer to Sets 1 and 2 as the recharged and neutral experiments, respectively. Initially, the recharged set has a farther extended warm pool (Figures 1a and 1b) and a slightly warmer cold tongue (not shown). Each experiment lasts 2 years.

Within each set, 10 pairs of (control and perturbed) ensemble members share the same initial ocean state but have slightly different initial atmospheric conditions. The perturbed experiments start with the same initial conditions as in the control experiments but include a superimposed westerly wind anomaly (the same in all perturbed experiments; Figure 1c) added to the model-generated wind stress in the tropical Pacific. For comparison, we use data from the Simple Ocean Data Assimilation (SODA), Version 2.2.4 [*Carton and Giese*, 2008], hereafter referred to as the "observations."

The imposed wind stress anomaly matches the WWB observed in February-March 1997 [*Lengaigne et al.*, 2002], believed to be partially responsible for the strength of 1997/1998 El Niño. This intense WWB begins in mid-February and lasts for about 1 month. Although the effects of timing, structure, and duration of WWB are also important [e.g., *Fedorov*, 2002], they go beyond the scope of this study.

3. Calculating the Energetics

Following previous studies [*Brown et al.*, 2011; *Goddard and Philander*, 2000], we compute the two key variables in equation (1) as follows

$$W = \iint \vec{u} \cdot \vec{\tau} \, dA \qquad (3)$$

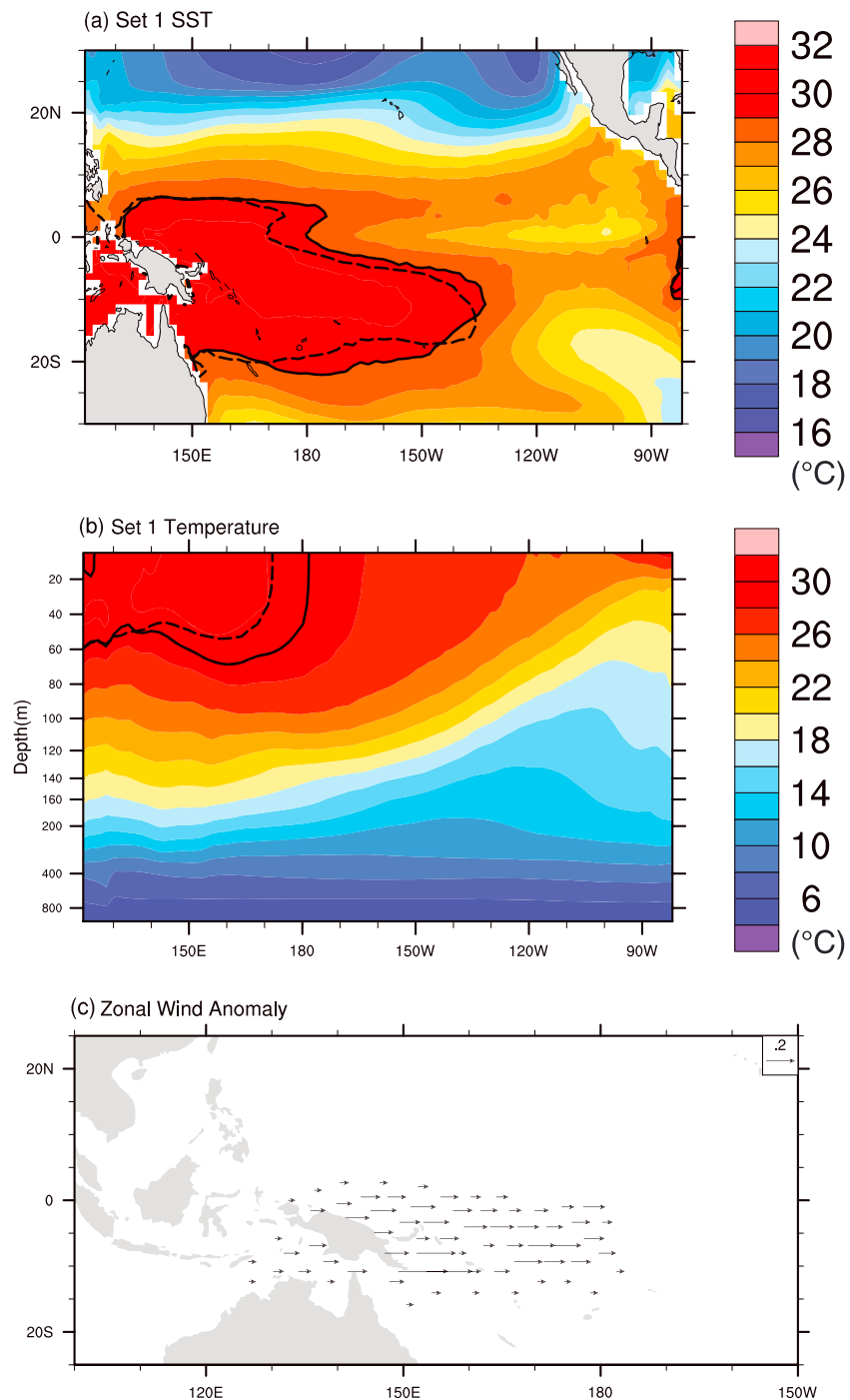$$E = \iiint \frac{\tilde{\rho}^2}{2S^2} \, dV \qquad (4)$$

Figure 1. (a and b) A comparison between model initial states in Sets 1 and 2. These two panels show SST and temperature as a function of depth along the equator (in °C) in February, when the WWB is applied, with the solid lines indicating the 29°C isotherm for Set 1. The dashed lines indicate the 29°C isotherm for Set 2. Note the greater extent of the warm pool in Set 1. (c) The spatial structure of the imposed westerly wind burst at its peak. The unit wind vector corresponds to 0.2 N/m^2. Note that the wind burst has a greater signature in the Southern Hemisphere. Reproduced from *Fedorov et al.* [2014].

where A denotes the area of the tropical Pacific basin (15°S–15°N, 130°E–85°W) and V denotes the volume of the tropical Pacific basin within 0–400 m. $\vec{\tau} = (\tau_x, \tau_y)$ is wind stress, and $\vec{u} = (u, v)$ describes surface currents; typically, the meridional contribution is neglected. Potential density, given by $\widetilde{\rho} = \rho - \rho^*(z)$, is calculated from temperature and salinity using a linearized equation of state for seawater [*Goddard and*

Philander, 2000], where $\rho*(z)$ is the time mean horizontal average over tropical Pacific basin, and $S^2 = -(1/g)\mathrm{d}\rho*(z)/\mathrm{d}z$.

In equation (4), $\widetilde{\rho}^2$ can be further decomposed as

$$\widetilde{\rho}^2 = \overline{\rho}^2 + 2\overline{\rho}\rho' + \rho'^2 \tag{5}$$

by splitting $\widetilde{\rho}$ into a climatology component $\overline{\rho}$ and a perturbation component ρ'. Substituting equation (5) into equation (4), one obtains three corresponding terms—mean energy E_{mm}, mean perturbation energy E_{mp}, and perturbation energy E_{pp} (supporting information). Similarly, one can split W into W_{mm}, W_{mp}, and W_{pp}. The model climatology is computed using the last 100 years of the spin-up run.

Following *Fedorov et al.* [2003], we use for analysis the mean perturbation terms (E_{mp} and W_{mp}), which dominate the time-varying parts of the expressions. Previous studies have shown that E_{mp} describes mean changes in thermocline slope: typically a positive (negative) E_{mp} indicates a thermocline steeper (flatter) than the climatology (supporting information; also see *Goddard and Philander* [2000]).

4. Results

The response of the coupled system to the same WWB turns out to be dramatically different in the two perturbed sets (Figures 2a and 2b). Without the WWB, the recharged set develops a moderate CP warming in about a year, while the neutral develops a weak La Niña (Figures 2c and 2d), as indicated by the ensemble means. However, when the WWB is imposed, the recharged set shifts into a strong EP event, while the neutral set slides into a weak CP event (Figures 2e and 2f). The simulated CP events are reminiscent of El Niño of 2002/2003 and 2004/2005, and the EP event resembles that of 1997/1998 (Figure S1 in the supporting information).

Differences in the system response to the WWB become especially clear if one computes anomalies of the perturbed runs relative to the control runs (Figure S2). Dynamical causes for these differences are discussed in *Fedorov et al.* [2014]. Here we will focus on the ocean energetics perspective.

E-W phase diagrams, arising from the ocean energetics, provide a clear illustration of the development of both warm and cold events. With the damping term in equation (1) relatively small, W is nearly proportional to the rate of change of E. Consequently, the system follows counterclockwise trajectories on the *E-W* diagrams in both sets of experiments (Figures 2a and 2b). Note that the Niño3-Ocean Heat Content diagrams are also frequently used to describe system phase evolution, but an advantage of the current approach is that it is based on energy conservation.

The downward APE excursions during warm events confirm the importance of thermocline variations for the both types of El Niño. Nevertheless, differences between the EP and CP events are striking (Figures 2a and 2b). The EP event (Set 1 Perturbed) exhibits a much more extended trajectory, with E_{mp} reaching very low values (Figures 2a and 2e). In contrast, the CP events (Set 1 Control and Set 2 Perturbed) are seen as relatively small loops; Set 1 Control has a stronger CP and hence reaches lower values of E_{mp} (Figures 2a–2c and 2f). The weak La Niña event in Set 2 Control, on the other hand, is associated with a positive E_{mp} near the end of the first year (Figures 2b and 2d).

It is noteworthy that the initial impact of the superimposed WWBs in both sets is seen as a rapid reduction in W_{mp} but accompanied by a relatively small change in E_{mp}, which is similar to the result of *Fedorov* [2002] obtained with an intermediate coupled model; subsequent negative anomalies in W_{mp} correspond to the strengthening of the Bjerknes feedback involving zonal winds and the east-west SST gradient in the tropical Pacific. The *E-W* diagrams also highlight the importance of the ocean initial state to the development of the coupled system: Set 1 starts with a smaller initial E_{mp} (flatter thermocline) and W_{mp} (weaker westward surface currents and trade winds) as compared to Set 2 (Figures 2a and 2b). This difference allows Set 1 to generate warmer events (greater negative values of E_{mp}) than Set 2 does, which further illustrates equation (2).

That *E-W* trajectories indeed describe the evolution of the coupled system is confirmed by the fact that E_{mp} provides a good proxy for the SST anomaly in the eastern equatorial Pacific even on monthly timescales (Figure 3), not just on interannual timescales as reported by previous studies [*Brown et al.*, 2011; *Fedorov*, 2007; *Goddard and Philander*, 2000]. Five day mean results show that E_{mp} is anticorrelated with the Niño3
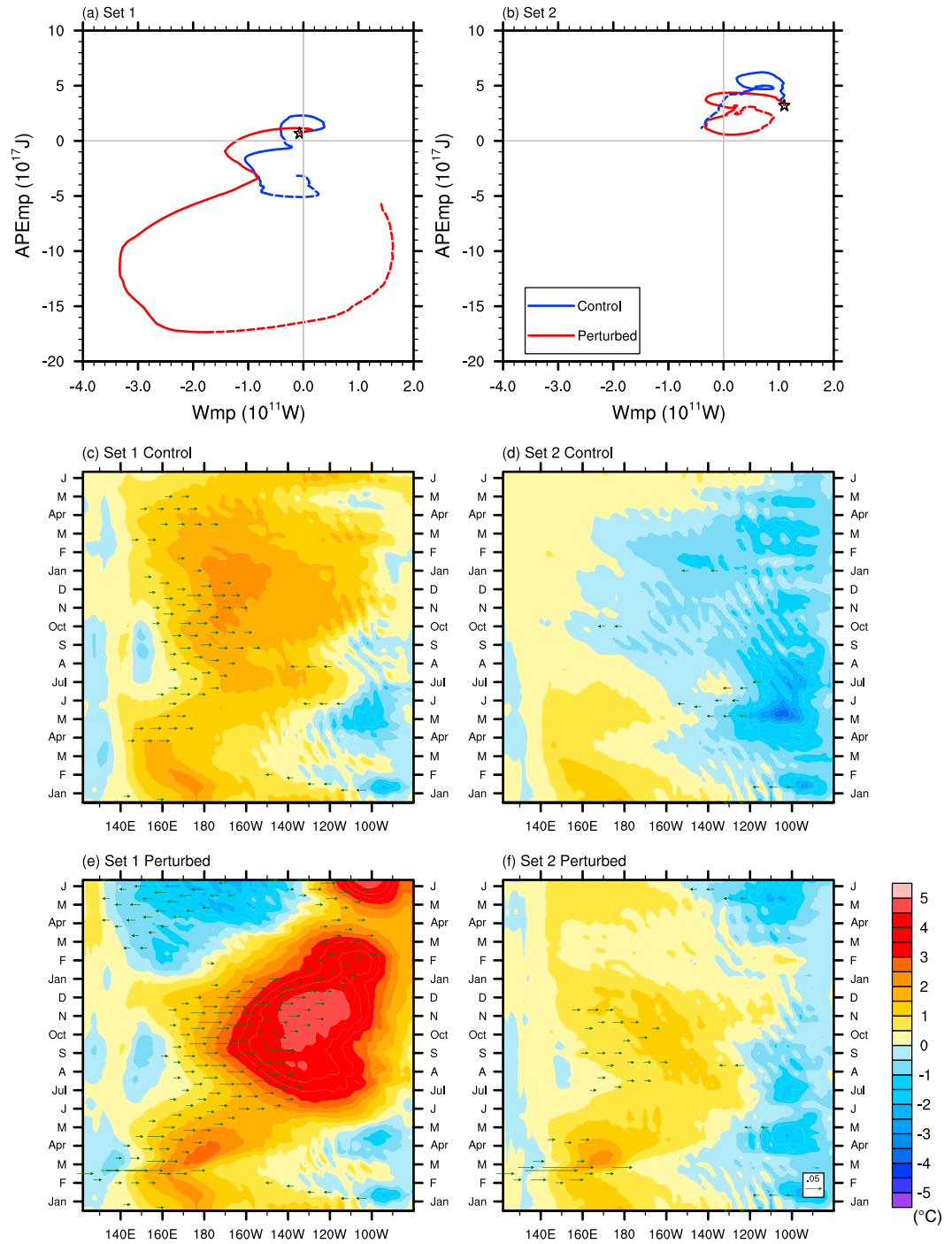
Figure 2. (a and b) *E-W* phase diagrams for Sets 1 and 2. Ensemble mean trajectories for the control and perturbed cases are shown as blue and red lines, respectively. A 2-month running mean is applied. Solid lines indicate the first year, while the dashed lines indicate the first half of the second year. The stars represent the beginning of the first year. Warm events are associated with counterclockwise loops lowering the APE of the system. Hovmoller diagrams for ensemble mean equatorial SST anomalies (colors) in °C for (c) Set 1 Control, (d) Set 2 Control, (e) Set 1 Perturbed, and (f) Set 2 Perturbed, reproduced from *Fedorov et al.* [2014]. The superimposed arrows represent the corresponding zonal wind stress anomalies, with values smaller than 0.02 N/m^2 removed. The unit wind vector corresponds to 0.05 N/m^2. Variables are averaged within the equatorial band 2°S–2°N.
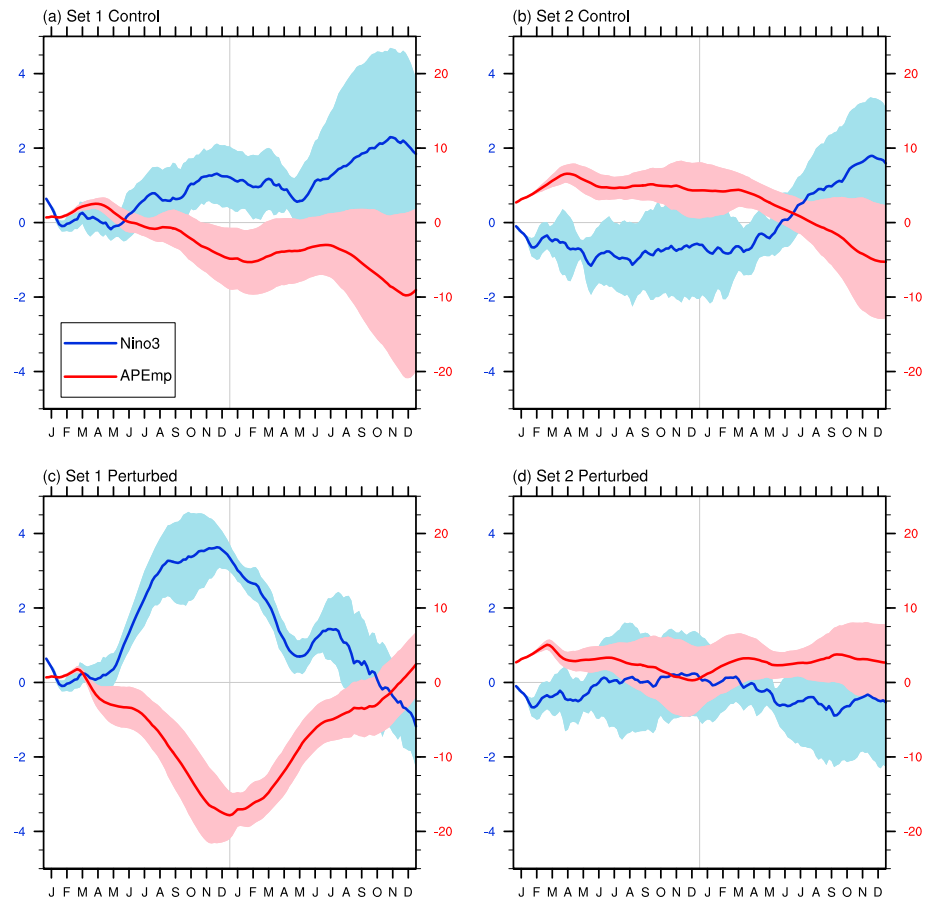
Figure 3. The Niño3 index and APE variations for (a) Set 1 Control, (b) Set 2 Control, (c) Set 1 Perturbed, and (d) Set 2 Perturbed. Color lines indicate ensemble mean values; shading indicates the corresponding standard deviation interval. Note the strong anticorrelation between the two variables. Hereafter, only the E_{mp} term is used for the APE.

index during both El Niño and La Niña events (the correlation coefficient is as high as -0.8 or -0.9), with the Niño3 index leading E_{mp} by about 1 month. Although only the ensemble mean results are shown here, the high anticorrelation also holds for each individual member, so that a negative (positive) E_{mp} is always accompanied by a warm (cold) Niño3 anomaly.

Further, looking at the individual members of these experiments (40 total) reveals a broad continuum of simulated warm and cold events, generally consistent with the observations (Figure 4a). It is important that even within each experimental set, there are large differences between ensemble members, especially in the neutral sets. Therefore, to investigate the robustness of main results in Figure 4, we have computed ensemble means and standard deviations for each set (Figure S3).

Let us consider, for example, the Niño4 and Niño3 indices and their relationship at the peak of the events (Figure S3a). In the recharge set, the warm events are clearly significant with Niño4 or Niño3 index much higher than the typical threshold 0.5°C. The neutral set looks more uncertain. The CP event is marginally significant with a probability of about 80% that Niño4 index would exceed 0.5°C. The weak La Niña event, however, harbors a larger uncertainty with a significant probability of neutral conditions. Nevertheless, this uncertainty does not affect our conclusions since the distinction between the EP and CP events is quite robust (Figures S3a, S3b, and S3d).

Next, we consider E_{mp} and SST anomalies at the peak of the events. The strong anticorrelation between E_{mp} and the Niño3 SST anomalies persists in both our experiments and the observations for a broad range of warm and cold events, resulting in a nearly linear relationship between the two variables (Figure 4b). However, the connection between E_{mp} and central Pacific SST anomaly (Niño4) is more complicated. For
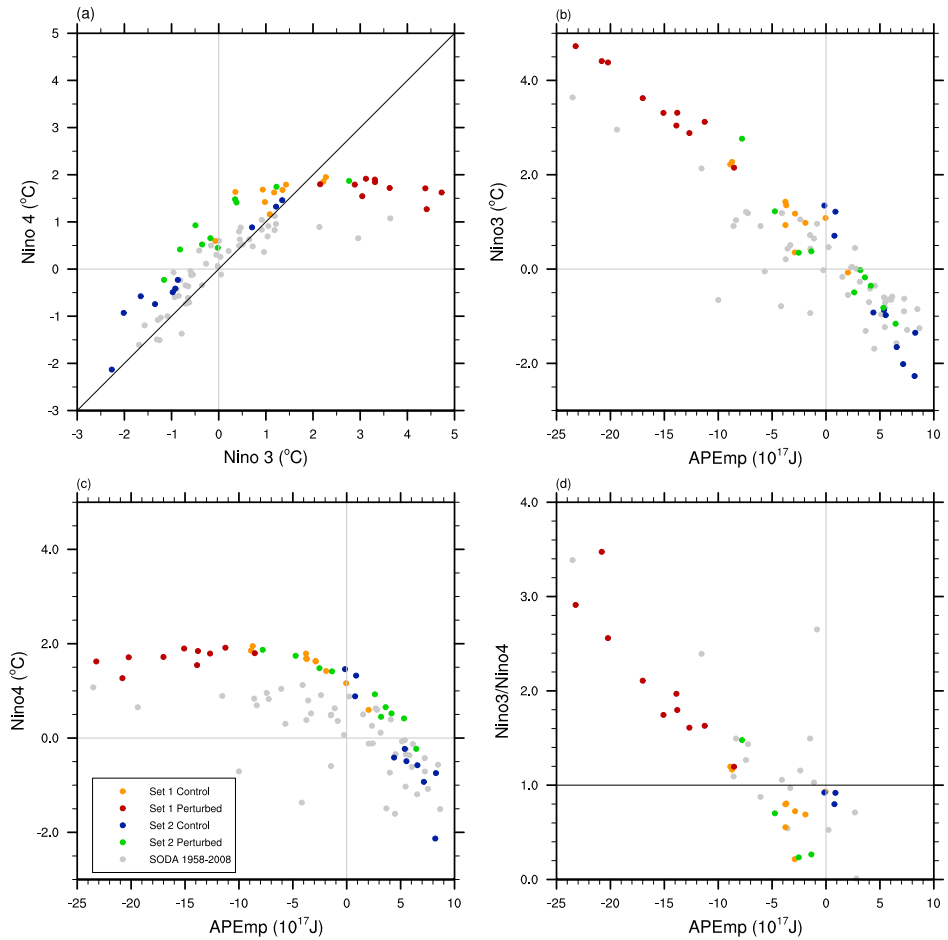
Figure 4. (a) The Niño4 versus Niño3 index; (b–d) the Niño3 index, the Niño4 index, and the ratio Niño3/Niño4 versus the APE, all at the peak of events. We use October-November-December mean values for the model ensemble members (colored dots) and November-December-January mean values for the observations (gray dots, based on SODA). Note the general agreement between the model and the observations. Figure 4a is partly reproduced from *Fedorov et al.* [2014]. Only warm events, with both Niño indices being positive and either one exceeding 0.5°C, are shown in Figure 4d.

stronger El Niño events, Niño4 stays at a saturated level (Figure 4c), but for cold and weaker warm events, E_{mp} and Niño4 SST are roughly anticorrelated (Figure 4c) but with a large spread.

Subsequently, E_{mp} allows us to quantify the diversity of El Niño events. Selecting all warm events (i.e., with both Niño3 and Niño4 indices positive, and either one greater than 0.5°C) and computing the ratio Niño3/Niño4 reveal a high anticorrelation between E_{mp} and this ratio in both the model and the observations (Figure 4d). That is, E_{mp} at the mature phase of warm events offers a good indicator for the El Niño type. Specifically, higher negative values of E_{mp} correspond to higher Niño3/Niño4 ratios and therefore more EP-like warmings. In contrast, lower negative values of E_{mp} correspond to smaller Niño3/Niño4 ratios and therefore CP El Niño events.

Another important finding is that WWBs enhance the predictability of the system development, if APE serves as a predictor. The E_{mp} before the imposed WWBs, in both the recharged and neutral sets, shows almost no ability to predict the Niño3 index at the peak of events (Figures 5a and 5c). However, in both perturbed sets, E_{mp} after WWBs (during the last week of March) is anticorrelated with the Niño3 at the warming peak (dots falling onto one line in Figure 5d), suggesting a much higher predictability of the system after the burst than in the control sets (Figure 5b). This result is further demonstrated by computing correlations between the initial E_{mp} and wintertime Niño3 SSTs for each of the sets. These correlations increase in the perturbed sets after the WWB timing, especially in the recharged set, but barely change in the
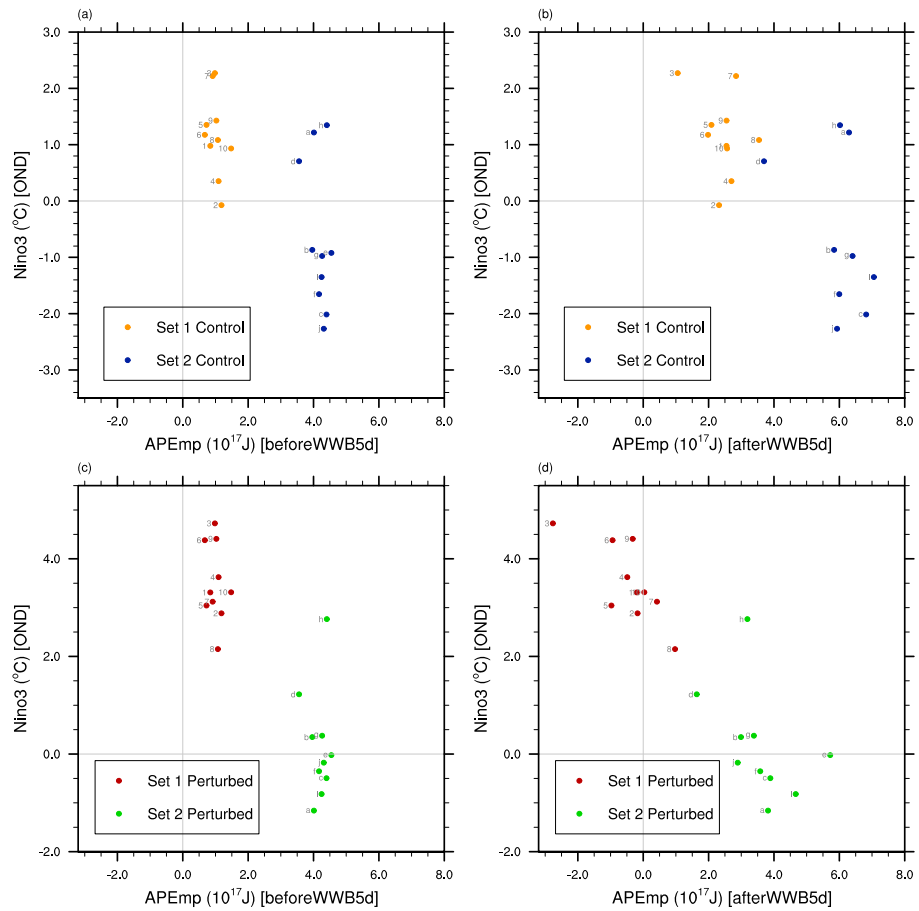
Figure 5. The Niño3 index at the end of the year versus the APE at the start of the year. The APE is estimated just (a and c) before or (b and d) after the time of the WWB. Here "before" and "after" the WWB mean 5 day averages for 11–15 February and 26–30 March, respectively. Figures 5a and 5b show control cases and Figures 5c and 5d show perturbed cases. Note the improved predictability of the system development after the WWB was imposed as dots in Figure 5d fall tightly onto one line (also Table S1). The Niño3 index is averaged for October-November-December.

control sets (Table S1). That is, after a strong WWB, the ocean thermocline contains more information to predict the incoming warm event, even before the spring predictability barrier.

One could try using the Niño3 index, rather than the APE, to conduct such assessment, but would find a significantly worse predictability due to the spring predictability barrier in SST persistence. Why is then the APE works better than the Niño3 index as a predictor, especially when the Niño3 index and the APE are anticorrelated and the former leads the latter by 1 month? The critical reason is that the APE describes the state of the equatorial thermocline. Right after the imposed WWB, the thermocline has been already affected in the western and central Pacific and has much more information about the system subsequent development than the SST.

5. Conclusions

Our work demonstrates that ocean energetics is a useful diagnostics tool for studying the impact of WWBs on the development, diversity, and predictability of El Niño events. The APE, a key variable characterizing the tropical thermocline, is shown to offer a good proxy for SST anomalies in eastern equatorial Pacific on interannual and even monthly timescales. In particular, *E-W* phase diagrams offer a clear illustration for the development of different types of El Niño events, with the size of the loops related to the type of generated warming. Moreover, in our experiments and in the observations, there seems to be an APE threshold—for the APE anomalies stronger than this threshold, an EP warming develops; for weaker anomalies, typically

only a CP warming is possible. It is important, however, that the transition between the two types of events is actually gradual and involves a strengthening of the thermocline feedback that gives rise to greater APE anomalies.

Although the APE and the Niño3 index are anticorrelated, they are different, albeit complementary, characteristics of the coupled system—the Niño3 index is based on SST anomalies averaged over the eastern equatorial Pacific (5°S–5°N, 150°W–90°W), while the APE is based on subsurface density variations in the entire tropical Pacific domain (15°S–15°N, 130°E–85°W, 0–400 m). The Niño3 index provides more information on surface conditions (especially important for the state of the atmosphere). In contrast, as an integral measure over the entire tropical Pacific basin, the APE provides much more information on the state of the ocean thermocline that carries the long-term memory of the coupled system.

Consequently, the APE is a better predictor of the system development and reveals that a timely WWB can enhance the predictability of the system development. This is evident from the tight linear relationship between the APE computed just after the wind burst and the Niño3 index computed at the peak of the events. This relationship emerges only in the perturbed experiments and connects the APE in March and the wintertime Niño3 index despite the spring predictability barrier. Thus, although in general intraseasonal variability limits the predictability of ENSO [e.g., *Fedorov et al.*, 2003; *Kleeman*, 2008; *Levine and Jin*, 2010], strong WWBs that happen at a certain time of the year can make the system development more predictable.

References

Ashok, K., S. K. Behera, S. A. Rao, H. Y. Weng, and T. Yamagata (2007), El Niño Modoki and its possible teleconnection, *J. Geophys. Res.*, *112*, C11007, doi:10.1029/2006JC003798.

Brown, J. N., and A. V. Fedorov (2010), How much energy is transferred from the winds to the thermocline on ENSO time scales?, *J. Clim.*, *23*(6), 1563–1580.

Brown, J. N., A. V. Fedorov, and E. Guilyardi (2011), How well do coupled models replicate ocean energetics relevant to ENSO?, *Clim. Dyn.*, *36*(11-12), 2147–2158.

Burls, N. J., C. J. C. Reason, P. Penven, and S. G. Philander (2012), Energetics of the tropical Atlantic zonal mode, *J. Clim.*, *25*(21), 7442–7466.

Cai, W., et al. (2014), Increasing frequency of extreme El Niño events due to greenhouse warming, *Nat. Clim. Change*, *4*(2), 111–116.

Carton, J. A., and B. S. Giese (2008), A reanalysis of ocean climate using Simple Ocean Data Assimilation (SODA), *Mon. Weather Rev.*, *136*(8), 2999–3017.

Clarke, A. J., and S. Van Gorder (1999), The connection between the boreal spring Southern Oscillation persistence barrier and biennial variability, *J. Clim.*, *12*(2), 610–620.

Fedorov, A. V. (2002), The response of the coupled tropical ocean-atmosphere to westerly wind bursts, *Q. J. R. Meteorol. Soc.*, *128*(579), 1–23.

Fedorov, A. V. (2007), Net energy dissipation rates in the tropical ocean and ENSO dynamics, *J. Clim.*, *20*(6), 1108–1117.

Fedorov, A. V., S. L. Harper, S. G. Philander, B. Winter, and A. Wittenberg (2003), How predictable is El Nino?, *Bull. Am. Meteorol. Soc.*, *84*(7), 911–919.

Fedorov, A. V., S. Hu, M. Lengaigne, and E. Guilyardi (2014), The impact of Westerly wind bursts and ocean initial state on the development, and diversity of El Niño events, *Clim. Dyn.*, doi:10.1007/s00382-014-2126-4.

Goddard, L., and S. G. Philander (2000), The energetics of El Nino and La Nina, *J. Clim.*, *13*(9), 1496–1516.

Harrison, D. E., and G. A. Vecchi (1997), Westerly wind events in the tropical Pacific, 1986–95*, *J. Clim.*, *10*(12), 3131–3156.

Kao, H. Y., and J. Y. Yu (2009), Contrasting Eastern-Pacific and Central-Pacific types of ENSO, *J. Clim.*, *22*(3), 615–632.

Karnauskas, K. B. (2013), Can we distinguish canonical El Niño from Modoki?, *Geophys. Res. Lett.*, *40*, 5246–5251, doi:10.1002/grl.51007.

Kessler, W. S. (2002), Is ENSO a cycle or a series of events?, *Geophys. Res. Lett.*, *29*(23), 2125, doi:10.1029/2002GL015924.

Kleeman, R. (2008), Stochastic theories for the irregularity of ENSO, *Philos. Trans. R. Soc. A*, *366*(1875), 2511–2526.

Kug, J. S., F. F. Jin, and S. I. An (2009), Two types of El Niño events: Cold Tongue El Niño and Warm Pool El Niño, *J. Clim.*, *22*(6), 1499–1515.

Lee, T., and M. J. McPhaden (2010), Increasing intensity of El Niño in the central-equatorial Pacific, *Geophys. Res. Lett.*, *37*, L14603, doi:10.1029/2010GL044007.

Lengaigne, M., and G. A. Vecchi (2010), Contrasting the termination of moderate and extreme El Niño events in coupled general circulation models, *Clim. Dyn.*, *35*(2-3), 299–313.

Lengaigne, M., J. P. Boulanger, C. Menkes, S. Masson, G. Madec, and P. Delecluse (2002), Ocean response to the March 1997 westerly wind event, *J. Geophys. Res.*, *107*(C12), 8015, doi:10.1029/2001JC000841.

Lengaigne, M., E. Guilyardi, J. P. Boulanger, C. Menkes, P. Delecluse, P. Inness, J. Cole, and J. Slingo (2004), Triggering of El Niño by westerly wind events in a coupled general circulation model, *Clim. Dyn.*, *23*(6), 601–620.

Lengaigne, M., J. P. Boulanger, C. Menkes, and H. Spencer (2006), Influence of the seasonal cycle on the termination of El Niño events in a coupled general circulation model, *J. Clim.*, *19*(9), 1850–1868.

Levine, A. F. Z., and F. F. Jin (2010), Noise-induced instability in the ENSO recharge oscillator, *J. Atmos. Sci.*, *67*(2), 529–542.

McPhaden, M. J. (1999), Genesis and evolution of the 1997–98 El Niño, *Science*, *283*(5404), 950–954.

McPhaden, M. J. (2003), Tropical Pacific Ocean heat content variations and ENSO persistence barriers, *Geophys. Res. Lett.*, *30*(9), 1480, doi:10.1029/2003GL016872.

McPhaden, M. J., and X. Yu (1999), Equatorial waves and the 1997–98 El Niño, *Geophys. Res. Lett.*, *26*(19), 2961–2964, doi:10.1029/1999GL004901.

Philander, S. G. (1990), *El Niño, La Niña, and the Southern Oscillation*, vol. 9, 293 pp., Academic Press, San Diego, Calif.

Ray, S., and B. S. Giese (2012), Historical changes in El Niño and La Niña characteristics in an ocean reanalysis, *J. Geophys. Res.*, *117*, C11007, doi:10.1029/2012JC008031.

Sarachik, E. S., and M. A. Cane (2010), *The El Niño-Southern Oscillation Phenomenon*, vol. 13, 369 pp., Cambridge Univ. Press, Cambridge, U. K., and New York.

Takahashi, K., A. Montecinos, K. Goubanova, and B. Dewitte (2011), ENSO regimes: Reinterpreting the canonical and Modoki El Niño, *Geophys. Res. Lett.*, *38*, L10704, doi:10.1029/2011GL047364.

Torrence, C., and P. J. Webster (1998), The annual cycle of persistence in the El Niño-Southern Oscillation, *Q. J. R. Meteorol. Soc.*, *124*(550), 1985–2004.

Yeh, S. W., J. S. Kug, B. Dewitte, M. H. Kwon, B. P. Kirtman, and F. F. Jin (2009), El Niño in a changing climate, *Nature*, *461*(7263), 511–U570.